Reports

Computer Graphic Display Method for Visualizing Three-Dimensional Biological Structures

JAVIER JIMÉNEZ, ANTONIO SANTISTEBAN, JOSÉ MARÍA CARAZO, JOSÉ L. CARRASCOSA

A computer graphic display method that produces two-dimensional perspective views of three-dimensional objects is presented. The method is applied to the reconstruction at a resolution of 2.2 nanometers of the neck of bacteriophage ϕ29, obtained from transmission electron micrographs processed by the direct Fourier method. The combined use of directed illumination, reflectance models, color, and different levels of transparency provides a powerful tool for a better interpretation of the three-dimensional structure, allowing improved correlation with genetic, structural, and biochemical data.

THE THREE-DIMENSIONAL (3-D) representation of objects is a critical step in structural analysis. X-ray crystallography and image-processing electron microscopic techniques have recently made possible the extraction of 3-D information from biologically relevant molecular assemblies. The increasing amount of information, derived from either protein crystals (*1*) or single particles (*2, 3*), demands reliable systems of representation for the interpretation of structure and for the correlation of structure with biological function.

We have studied the neck region of bacteriophage ϕ29, an area involved in viral morphogenesis. Bacteriophage ϕ29, a small DNA-containing virus that infects *Bacillus subtilis*, has a complex morphology (*4, 5*). The neck region was isolated and structurally analyzed by two-dimensional (2-D) Fourier filtering of electron micrographs of artificially induced 2-D crystals (*6–8*).

The 3-D structure of the ϕ29 neck was obtained by the application of Fourier-based methods to negatively stained 2-D neck crystals (*9*). The process of the 3-D reconstruction of the neck from its 2-D projections can be followed in Fig. 1. Figure 1A shows part of an original micrograph obtained in the transmission electron microscope; the arrangement of the individual necks in a hexagonal net, the crystal boundaries, and small defects are visible. The two images in Fig. 1B illustrate the data-acquisition process; we obtained a set of views in the electron microscope by means of a tilting stage; these views were filtered and used for the 3-D reconstruction by a direct Fourier method (*10–12*). Figure 1, C and D, shows the final 3-D object displayed in the form of sections by planes, either parallel or perpendicular to the crystal surface. The height of the reconstructed specimen is about 10 nm.

The 3-D architecture of the specimen is difficult to recognize in this display. Traditionally in electron microscopy, this problem has been solved by stacking transparent or wooden sheets in which consecutive sections of the model are either drawn or cut out. The construction of these models is awkward, and such models do not give a full 3-D idea of the structure, especially because a smooth surface joining the different sections is lacking. This is particularly true of those structures that have internal detail or those in which different density thresholds give rise to different descriptions of the object, which then must be compared. Examples of these problems are given below.

In recent years, computer graphic methods have been used to improve the quality of the representations (*13, 14*). Computer graphics has already been used for the same purpose in engineering design (*15*), medicine (*16*), and experimental fluid mechanics (*17*), and the underlying techniques are relatively well developed. They can be grouped into two general families. In the first (*18*), the model is seen as a 3-D array of small cubes (voxels), for each of which there is associated a density value. The display is computed directly from this array; in each case the system detects which voxels are visible from a given point of view and then uses them to compute the surface parameters needed for the representation. Our display method belongs to the second family (*19*), in which the outer surface of the model is detected a priori and is then used to construct the graphic output.

Assume that we want to display a solid surface defined by a given staining density on the particle represented by the sections in Fig. 1C. In our case, this surface was defined as that with the steepest density gradients. In each section, the equal density lines are isolated with a contour-following algorithm and are approximated by polygons (*20*), which are then joined by triangular tiles to form a surface satisfying some predefined smoothness criterion, usually to minimize the total lateral area of the model. This is the crucial step. An algorithm that generates the optimum tiling between two given polygons has been developed by Fusch *et al.* (*21*). The problem is to decide which pairs of polygons must be connected whenever a section contains several polygons. In simple cases this can be solved by pairing polygons whose centers of gravity are closest among all the possible pairs, and tapering to a point any unpaired polygon. However, some complicated models cannot be solved completely by this procedure, and manual interaction is required to solve the connectivity between sections. A tiled version of the model of the viral neck is shown in Fig. 2A (the maximum diameter is about 13 nm).

It is only necessary to construct the model once. The tiles are stored in disk and can be used to produce graphic representations or to generate new models in which the original solid is intersected by arbitrary planes. One builds the display by computing the representation on the screen for all the tiles, but updating only those points that contain information from parts of the model that are closer to the observer than points already considered (*19*). The intensity associated with each point is determined by the angles formed among the surface, the screen, and a point light source whose position can be controlled by the operator (*22*). We also use a "fade out" factor that decreases the light intensity linearly with the distance from the screen in such a way that points far from the observer are darker than those near him. The details of this "fade out" can also be controlled by the operator to provide the right amount of depth cuing. A display of the surface model of Fig. 2A is shown in Fig. 2B.

The whole process can be coded with relative efficiency. The model in Fig. 2A contains approximately 4500 triangular tiles, and its construction from individual sections takes 5 to 10 minutes of computer processing unit time in an IBM 370/158 computer. After that, the generation of each view consumes from 10 to 15 seconds.

There is an important problem in Fig. 2B: the inner details of the structure are masked by the outer surface and can be made visible only by cutting the model by an appropriate

J. Jiménez and A. Santisteban, IBM Madrid Scientific Center, Paseo Castellana 4, 28046 Madrid, Spain.
J. M. Carazo and J. L. Carrascosa, Centro de Biología Molecular, Consejo Superior Investigaciones Científicas, Universidad Autónoma, 28049 Madrid, Spain.

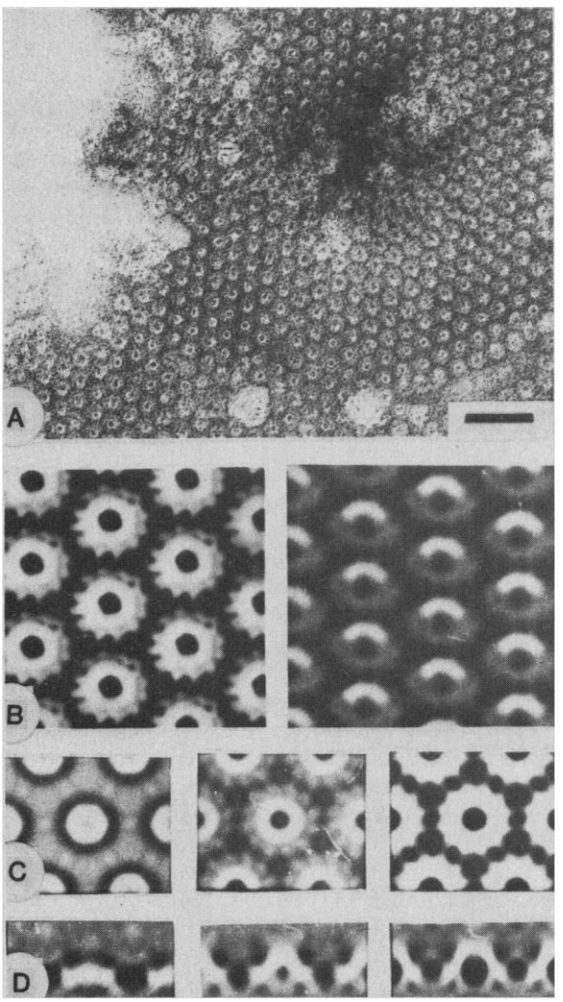

Fig. 1. Three-dimensional reconstruction process of the neck of bacteriophage ϕ29. (A) Transmission electron micrograph of the neck crystal; bar represents 50 nm. (B) Untilted and tilted (45°) images of the same crystal after Fourier filtering; the distance between neighboring specimens is about 15 nm in the untilted image. (C and D) Sections of the 3-D reconstruction of the specimen obtained from 30 tilted images. Sections are by planes parallel (C) and perpendicular (D) to the crystal surface. The spatial resolution in the reconstruction is 2.2 nm.

plane. However, when this is done, the relation of the inner detail to the outer surface is lost. An alternative method is to use translucent models to show the inner and outer structures at the same time. Such models are easily constructed by the display of only a given fraction of the pixels representing their surfaces. This fraction should change with the inclination of the surface with respect to the screen, so that faces that are seen "edge on" look denser than those that are perpendicular to the line of sight. A suitable simple rule is that, if the transparency is defined by skipping a fraction β of the pixels in faces that are perpendicular to the observer, faces whose normals are inclined by an angle Θ with respect to the line of sight should be drawn by skipping a smaller fraction, $\beta \cos \Theta$. Since pixels that are not displayed do not update the depth buffer, the rear parts of the model show through the gaps in the display of the front faces. The result (Fig. 2C) shows not only the outer surface of the viral neck but also an inner channel, with an overall conical shape, that runs for about 8 nm starting from the thicker end. The existence of this channel is important in understanding the interactions between the viral neck and the DNA.

Another problem is that the shape of the solid representing an object may depend on the density level chosen to define its surface. The 3-D image used in this work was obtained by averaging over as many as 50 to 60 individually constrasted images (*9*). The final result has a signal-to-noise ratio of 25 db, and it is possible to define different density levels, related to different probabilities of stain penetration, with confidence. Another view of the same viral particle at a higher density threshold, selected to represent the most contrasted areas that would still result in a connected structure, is shown in Fig. 2D. The model now contains 12 isolated regions, divided into two sets. The upper set is formed by six identical proteins, one per region, and each of the regions in the lower set is probably associated with two protein subunits, different from the ones above (*5–7*), with a strong twist near the section where the external surface of the specimen becomes larger.

An interesting possibility is to show in the same representation two surfaces corresponding to different density levels (cover). The outer surface is translucent and is superimposed on the inner opaque surface and in a different color. The formalism of the display can handle the superposition without any special precautions. A comparison of Fig. 1, C and D, and Fig. 2, B and D, shows how powerful these computer graphic display techniques are at providing suggestive images of complex 3-D objects.

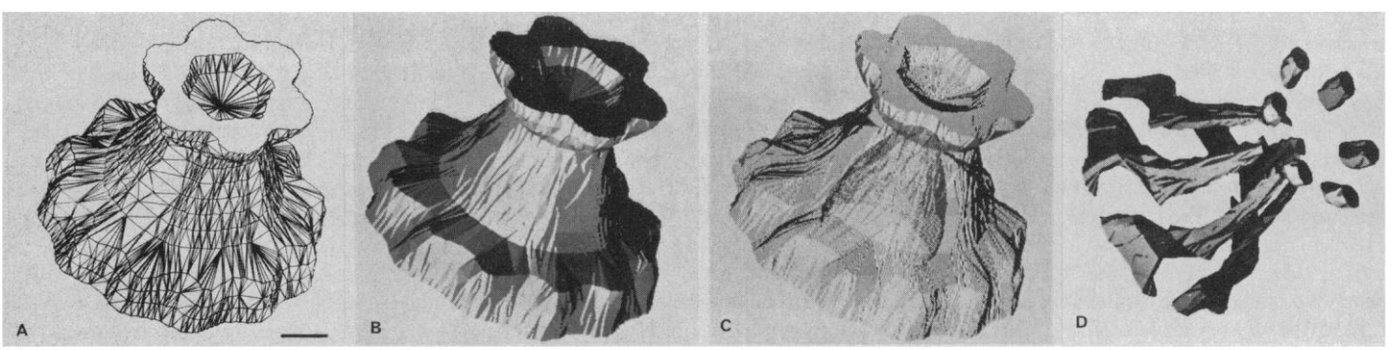

Fig. 2. Computer perspective views of the 3-D reconstructed neck of bacteriophage ϕ29. Bar represents 2.2 nm. Data are the same as in Fig. 1, C and D. (A) Tiled version of the model of the viral neck. (B) Surface model obtained by use of a low-density threshold level; the specimen shows a thick end, about 13 nm in diameter, narrowing to 7 nm at the opposite end. (C) Translucent representation of the same model, showing both inner and outer detail. (D) Model obtained with a higher density threshold level. It probably represents the backbones of the protein subunits; note the twist of the subunits where the external profile becomes larger.

REFERENCES AND NOTES

1. S. D. Fuller, *Methods Cell Biology* **22**, 251 (1981).
2. V. Knauer, R. Hegerl, W. Hoppe, *J. Mol. Biol.* **163**, 409 (1983).
3. A. Verschoor, J. Frank, M. Radermacher, T. Wagenknecht, M. Boublik, *ibid.* **178**, 677 (1984).
4. D. L. Anderson, D. D. Hickman, B. E. Reilly, *J. Bacteriol.* **91**, 2081 (1966).
5. J. L. Carrascosa, E. Méndez, J. Corral, V. Rubío, G. Ramirez, E. Viñuela, M. Salas, *Virology* **111**, 401 (1981).
6. J. L. Carrascosa, E. Viñuela, N. García, A. Santisteban, *J. Mol. Biol.* **154**, 311 (1982).
7. J. L. Carrascosa, J. M. Carazo, N. García, *Virology* **124**, 133 (1983).
8. J. M. Carazo, N. García, A. Santisteban, J. L. Carrascosa, *J. Ultrastruct. Res.* **89**, 79 (1984).
9. J. M. Carazo, A. Santisteban, J. L. Carrascosa, *J. Mol. Biol.* **183**, 79 (1985).
10. D. J. De Rosier and A. Klug, *Nature (London)* **217**, 130 (1968).
11. G. T. Herman, *Image Reconstruction from Projections* (Academic Press, New York, 1980).
12. S. X. Pan and A. C. Kak, *IEEE Trans. Acoust. Speech Signal Process.* **ASSP-31**, 1262 (1983).
13. M. Radermacher and J. Frank, *J. Microsc. (Oxford)* **136**, 77 (1984).
14. K. Namba, D. L. D. Caspar, G. J. Stubbs, *Science* **227**, 773 (1985).
15. A. A. G. Requicha and H. B. Voelcker, *IEEE Comput. Graph. Appl.* **CGA-3**, 25 (1983).
16. E. J. Farrell, R. Zapulla, W. C. Yang, *ibid.* **GGA-4**, 5 (1984).
17. J. Jiménez, M. Cogollos, L. Bernal, *J. Fluid Mech.* **152**, 125 (1985).
18. G. T. Herman and H. K. Liu, *Comput. Graph. Image Process.* **9**, 1 (1979).
19. J. D. Foley and A. Van Dam, *Fundamentals of Interactive Computer Graphics* (Addison-Wesley, Reading, MA, 1982).
20. J. Jiménez and J. L. Navalon, *IBM J. Res. Dev.* **26**, 724 (1982).
21. H. Fusch, Z. M. Zedem, S. P. Uselton, *Commun. ACM* **20**, 693 (1977).
22. B. T. Phong, *ibid.* **18**, 311 (1975).
23. This work was supported in part by the Fondo de Investigaciones Sanitarias and the Comisión Asesora para la Investigación Científica y Técnica.

19 March 1985; accepted 17 December 1985

The Discovery of Dust Trails in the Orbits of Periodic Comets

MARK V. SYKES, LARRY A. LEBOFSKY, DONALD M. HUNTEN, FRANK LOW

Analysis of data from the Infrared Astronomical Satellite has yielded evidence for narrow trails of dust coincident with the orbits of periodic comets Tempel 2, Encke, and Gunn. Dust was found both ahead of and behind the orbital positions of these comets. This dust was produced by the low-velocity ejection of large particles during perihelion passage. More than 100 additional dust trails are suggested by the data, almost all near the detection limits of the satellite. Many of these dust trails may be derived from previously unobserved comets.

THE INFRARED ASTRONOMICAL SATellite (IRAS) was launched on 26 January 1983 with the primary mission of mapping the sky at thermal infrared wavelengths and making observations while pointed toward particular objects of astrophysical interest (*1*). Four broad-band filters, having effective wavelengths of 12, 25, 60, and 100 μm, were used. IRAS was placed into a near-polar orbit whose plane was perpendicular to the Earth-sun line. As it orbited Earth every 103 minutes, its array of detectors swept out a strip 0.5° wide on the sky. The orbital precession rate of ~1° per day maintained the Earth-sun-satellite angle of ~90°. "Looking" straight out from Earth, IRAS would have mapped most of the sky in 6 months. To increase the rate of sky coverage, the orientation of IRAS was continually shifted by 0.25° in ecliptic longitude from orbit to orbit (*2*). This shifted the image of the sky by half the width of the detector array on each successive orbit. Consequently, the same location of sky was observed twice, over two consecutive orbits. This was designated as an "hours-confirmed" observation or HCON.

The mission was structured so that increasing ecliptic longitudes were observed over a period of about a week, and then the same region of the sky was rescanned the following week. This pattern was maintained over the first 7 months of the mission so that a given sky location was observed a total of four times. The first week and second week periods were designated the first and second HCON's, respectively. Over the remaining 3 months of the mission, a third HCON was obtained over most of the sky.

The observational strategy allowed for the study of extended solar system structures, such as the zodiacal emission, and also allowed for parallactic observations of solar system objects with Earth's orbital diameter, or a portion thereof, used as a baseline. This procedure was necessary to identify and accurately model the extended emission from solar system dust. The accurate study of extended emission from sources beyond the solar system (such as the galactic cirrus) requires that the effects of solar system dust be removed.

The final data products included three sets of sky flux maps, corresponding to the three HCON's, in which the sky was divided into 212 plates measuring 16.5° on a side (to allow for some overlap). These plates were constructed by pasting together individual scans of the sky from a given HCON and binning them into pixels ~2 arc minutes square (*3*). Typically, the scans used were taken over a period of weeks.

While analyzing the IRAS sky flux maps generated from the first HCON, we found trails of dust extending across many of the 16.5° plates. These trails appeared to be very narrow (a few pixels or less) and linear. Some extended completely across the plates, but most were shorter, on the order of 10° or less in apparent length. Two of the brightest trails (Fig. 1) were found to coincide with the projection on the sky of the orbits of comets Tempel 2 and Encke. A fainter trail contained comet Gunn (Fig. 2).

Jaggedness and breaks in the trails are due to data binning and changes in viewing from scan to scan. The greater the time between adjacent scans within a plate, the greater the parallax of the trail orbits. Thus, across some plates a trail may appear to break and to be angularly displaced.

The trails were identified by visual inspection of the lower bits of many of the first HCON images, without the benefit of spatial filtering (which, when properly tuned, would greatly enhance their contrast). The surface brightness of these trails was comparable to or much less than scan-to-scan variations in background brightness. This was also true with respect to noise levels in-scan. The fact that the dust trails were seen, in most cases, is due to the ease with which the eye can pick out a line of weak signal in an otherwise noisy image.

Determining the precise instantaneous length of a dust trail is hampered by the restricted viewing geometry (solar elongation ~90° ± 30°) and by the motion of the dust particles that make up the trails in their orbits over the period covered by the scans that compose an individual plate. Over a period of weeks, dust trail particles may have moved several degrees. Since scans generally cover increasing longitudes with time, dust trails with particles moving in prograde orbits may appear artificially elongated on

M. V. Sykes, L. A. Lebofsky, D. M. Hunten, Lunar and Planetary Laboratory, University of Arizona, Tucson, AZ 85721.
F. Low, Steward Observatory, University of Arizona, Tucson, AZ 85721.